Analytical Methods

Accepted Manuscript

Detection of cardiovascular drug and marine toxin using a multifunctional cell-based impedance biosensor system

Hongbo Li[1], Quchao Zou, Ling Zou, Qin Wang, Kaiqi Su, Ning Hu[1],*, Ping Wang*

Biosensor National Special Lab, Key Lab of Biomedical Engineering of Ministry of Education, Department of Biomedical Engineering, Zhejiang University, 310027 Hangzhou, China.

*Corresponding author: Tel.: +86 571 87952832; E-mail: cnpwang@zju.edu.cn (Ping Wang) huning@zju.edu.cn (Ning Hu)

[1] These authors contribute equally to this work

Abstract

With the growing concern on human health, relevant drug and food toxicity draws more and more attention. However, traditional methods like mouse bioassay cannot meet the sharply increasing demand of drug and food toxicity assessment. In this study, a multifunctional cell-based impedance biosensor system is established for drug and toxin analysis, using cell-based impedance biosensor (CIB) as the sensitive element. Cellular growth and beating experiments are carried out to verify the multifunction of the system. Four typical heart-related compounds including verapamil, bay K8644, chromanol 293B, and adriamycin are used for cardiotoxicity analysis function test of CIB system. Also, one typical marine diarrhetic toxin okadaic acid (OA) is used for cytotoxicity analysis function test of CIB system. From the results, the CIB system can reflect the drug function and toxicity by the cell growth and beating status directly. According to the results, the multifunctional CIB system may provide a high-throughput and utility method for effective screening of cardiovascular drug and marine toxin *in vitro*.

Keyword: cell-based impedance biosensor (CIB), cardiovascular drug, marine diarrhetic toxin, cytotoxicity

Introduction

Drug and food toxicity is a serious problem in the field of health care, pharmaceutical industry, and agriculture. Drug-induced cardiotoxicity is even more harmful among these. Cardiovascular side effect accounted for about 45% withdrawal of used drug and 30% attrition of drug [1-3], which is the main reason for drug withdrawal and development stop, so the cardiac safety assessment is taken seriously in the development, approval, and usage of drugs [4-9]. Besides, food plays a significant role in our daily life, so the food safety is also concerned by the public. For instance, biotoxins in the seafood have great damage to human health such as diarrhea, paralysis, and even death [10-12]. Consequently, early and efficient analysis methods are demanded to effectively assess drug and food toxicity.

Cell-based bioassay is a utility in vitro biological system in the research and application field in recent decades. Cells are used as the sensitive elements to sense the compound effect in the extracellular microenvironment. Compared with *in vivo* animal methods, *in vitro* cell-based bioassay can reflect the drug and food toxicity in a short term. However, the traditional cell-based bioassays (e.g. MTT method [13-15]) were end-point, complex, and harmful, which hampers the development of the cell-based bioassays. To exclude the disadvantages, Cell-based biosensor technologies are explored [16-24]. Cell-based biosensor can monitor the extracellular potential (by microelectrode array (MEA) and field effect transistor (FET)), acidification (by light addressable potentiometric sensor (LAPS) and FET), and impedance (by electrical cell-substrate impedance sensor (ECIS)) of cells cultured *in vitro*. Among these cell-based biosensors, ECIS is more similar with MTT for cell viability evaluation, which was first proposed by Giaever in 1984 [25]. In the last two decades, ECIS had been successfully applied to a number of cell behaviors, such as cell growth, cell proliferation, cell migration and invasion, cytotoxicity[25-33]. Most of cell behaviors are slow, so corresponding impedance sensor systems have a low temporal resolution, such as ECIS-Zθ [34-36]，Bionas 9600 adcon reader [37, 38] and automated multi-well setup [39]. However, some cells have a special behavior such as rhythmic beating of cardiomyocytes [40-44], and cardiomyocyte-based biosensor is a utility tool for cardiac safety assessment. Therefore, a multifunction detection system with a higher temporal resolution is demanded for cardiomyocyte-based impedance biosensor.

Official methods for marine toxins detection, such as paralytic shellfish poisoning (PSP) toxins, are the mouse bioassay (MBA) and the pre-column oxidation liquid chromatography with fluorescence detection (ox-LC-FLD)[45, 46]. However, the MBA method has low sensitivity and animal ethical problem while ox-LC-FLD method is limited by the expensive reference material and operation difficulty though its high sensitivity and reliability. Cell-based biosensor is a new approach in the field of drug and food toxicity assessment by monitoring the cell growth and cardiomyocyte beating non-invasively in a low-cost, high-throughput, and real-time way. Cell growth monitoring is capable of evaluating marine toxin which may have cytotoxicity to cells, such as okadaic acid (OA). Besides, to drug candidates which may induce cardiotoxicity of cardiomyocytes, cardiomyocyte beating monitoring provides a new approach for cardiac safety assessment. In this study, a multifunctional cell-based impedance biosensor system is established for drug and toxin analysis, providing both long-term and high-speed detection for cell growth and cardiomyocyte beating monitoring respectively. Fabrication of impedance sensor and system are introduced. The primary neonatal rat cardiomyocyte and neuro-2A cell line are employed to construct the cell-based biosensor for the cardiovascular drug and marine toxin analysis. All the details will be discussed in the following sections.

Experimental and methods

Working principle of cell-based impedance biosensor

Cell-based impedance biosensor (CIB) is an important biomedical method for cell biology research and disease diagnosis by monitoring living cells non-invasively and dynamically *in vitro*. Generally, a CIB unit consists of interdigitated electrodes (IDEs), culture wells, living cells and printed circuit board. Many researches have been focused on the simulation modeling of IDEs. As is shown in **Fig. 1**(A), it is an equivalent circuit model of IDEs[47, 48]. The model can be simplified in the cell-free situation (**Fig. 1**(B)). Also, the equivalent circuit model of two branches IDEs with cells can be presented as **Fig. 1**(C). As is reported in the former studies [47, 49, 50], the frequency response diagrams of cell-covered and cell-free IDEs are divided into four parts by three key frequencies f_{low}, f_{middle}, and f_{high}. Between f_{low} and f_{high}, the sensor has the high sensitivity which is generally between 5-50 kHz[48].

Fig. 1

As is described above, CIB mainly monitors the physiological status of living cells[51]. As shown in **Fig. 1**(D), IDEs are applied on a low sinusoidal voltage, and then the stable ion current is formed between the IDEs. When the surface of IDEs is cell-free, the impedance Z_0 reflects the baseline impedance. After the cells are cultured on the IDEs surface, the ion current is impeded with the increasing impedance value. Generally, the impedance value is normalized by cell index (CI) value, which is the ratio of the cell impedance change ΔZ to the baseline impedance value Z_0. CI value is an arbitrary unit and reflection of cell number, morphology, and attachment. In this way, CIB is able to monitor the growing status and reflect the external stimuli on cells in real time.

Besides, CIB can monitor some cells with special behavior. For example, Cardiomyocytes can generate rhythmic beating based on excitation-contraction (E-C) coupling. E-C coupling describes the physiological process of converting an electrical stimulus to a mechanical response[52]. During the process, movement of calcium ion, which is the key factor of E-C coupling, results in the cardiac relaxation and contraction and finally results in the changes of cell morphology and cell attachment (**Fig. 1** (E)). For monitoring these changes, the high-speed biosensor system is demanded.

Sensor fabrication and instrument design

For CIB fabrication (**Fig. 2**(A)), 300 nm Au layer is fabricated on the glass substrate as metal electrodes, while 30 nm Cr layer used to enhance the adhesion of

Au and glass. Subsequently, the electrode and lead patterns of CIB are formed through etching after photolithography. A CIB chip has 16 IDEs. As is shown in **Fig. 2**(B), diameter of each IDEs is 5 mm and their branches consist of small circle electrodes with diameter of 90 μm. The coverage of IDEs is about 60%. For cell culture, a sensor chamber custom-made with 16 wells is fixed on the CIB chip.

Fig. 2

The detection instrument of CIB consists of three modules, cell-based impedance biosensor units, hardware module, and data processing module. The entire instrument platform is illustrated in **Fig. 2**(C). CIB unit has been described above. The hardware module contains signal generator module, current-to-voltage converter module, amplification module, filter module, and the data acquisition module. The data acquisition module is a National Instruments USB-6255 16-Bit, M Series Multifunction DAQ with a high-speed rate of 1.25 MS/s. The impedance measurement ranges from 50Ω to 1kΩ. When the system starts to work, multifunction DAQ card creates a continuous low-voltage signal (20Vrms, 10 kHz) applied on the CIB unit. An ion current signal is generated between IDEs. Then the current-to-voltage converter module turns the current signals into voltage signals. After amplification and filtering, the signals can be sampled by DAQ card which converted voltage signals into digital signals for further processing and analysis. For each round of detection process, 20 s data is recorded for high-speed detection (f_s = 250 kHz) and a single point is calculated by 20 s data for long-term detection.

Cell culture

For cell experiments, rat cardiomyocytes and Neuroblastoma cells (Neuro-2a) (American Tissue Culture Collection, CCL131) are employed. For cardiomyocytes, the sensor plates are coated with gelatin overnight in 4℃ refrigerator and rats are sterilized by 75% alcohol before experiments. Rat chest wall was cut, and the heart is rapidly excised from neonatal rat by Dulbecco's modified Eagle medium (DMEM). Atriums are removed from the hearts. Ventricles are left and moved into a bottle with 2 ml Hanks balanced salt solution (HBSS) inside. Then ventricles are shredded into tissue fragments. After removing HBSS, tissue fragments are digested by trypsin and collagenaseⅡ. The fragments are blown using a glass pipette to aspirate supernatant and moved into another tube with 10% Fetal Bovine Serum (FBS) DMEM to stop digestion. Cell suspension is centrifuged with 800 rpm for 5 min after that suspension was abandoned. After resuspending the cells with 4 ml DMEM (10% FBS), cells are derived and cultured in sensor wells and maintained at 37 ℃ in an incubator with 5% CO_2. The medium are changed every 24 h.

Subsequently, Neuro-2a cells are purchased from ATCC. Before seeding cells on the sensor, the sensor wells are incubated with 5 μg/mL laminin in 0.01M phosphate buffer solution (PBS, pH=7.4) for 1 hour at 37 °C to improve the adhesion of cells onto sensors. After that, Neuro-2a cells are resuspended in 1 ml culture medium (1% penicillin: Hyclone, cat. SV30010, 10% fetal bovine serum: Gibco, cat. 16000-044, Dulbecco's modified eagle medium (DMEM): Hyclone, cat. SH30022.08). Then cell suspension was transferred to the sensor wells and maintained at 37 ℃ in an incubator with 5% CO_2. The medium are also changed every 24 h.

Results and discussion

Performance testing of sensor and instrument

The stability of the CIB unit and system is of great importance for following bioassay and further analysis. The coefficient of variation (CV) is a common parameter to reflect the stability of the sensor and detection instrument. Since the impedance of the CIB with cell usually varies from tens to hundreds, 50 Ω to 1000 Ω is chosen as the detection range for linear calibration **(Fig. 3**(A) and (B)). The CV values of 50 Ω test are within 0.13% while the CV values of 1000 Ω test are within 0.56% for long-term detection. Moreover, stability of a CIB unit is tested with 200 μL phosphate buffer solution (PBS, pH=7.4) (**Fig. 3** (C)). The deviation of the CIB unit is within ±0.05 for long-term detection and ±0.005 for high-speed sampling which make it available for cellular growth and beating experiments.

Fig. 3

Optimization of CIB unit

As is described above, living cells play a significant role in CIB unit. The initial seeding density, which is the important parameter to establish a CIB, strongly influence the growth or beating of cells, and the sensitivity of CIB unit. We inoculated Neuro-2a cells into sensor wells at density of 1k, 5k, 10k, 20k, 30k, 50k and 60k cells/well and began the long-term detection for the whole experiment by our CIB detection instrument. The cellular growth curves of Neuro-2a cells with different densities are displayed in **Fig. 4**. Each cellular growth curve shows the average and standard deviation of the CI values. The CI values of "empty" wells keep close to zero during the whole long-term detection. During the beginning stage of cellular adhesion, all cellular growth curves represented density-related high increment speed. During the following growing stage, all cellular growth curves represented gentle rise in CI. After about 24 h, cellular growth curve at density of 60k, 50k, 30k and 20k cells/well decline gradually. While cellular growth curves at density of 1k and 5k cells/well increased too slowly to reach a high CI value even after 35h, which cannot satisfy the requirement of CIB. Therefore, 10k cells/well is chosen as the initial seeding density of Neuro-2a cells.

Cardiomyocytes can generate rhythmic beating caused by excitation-contraction coupling resulting in the changes of the cell morphology and cell attachment. The recording of cardiomyocytes beating is an important application of CIB. As is demonstrated above, the number of initial seeding cells influences the increasing rate of CI values seriously. Therefore, specifically for cardiomyocytes, we had experiments of seeding different densities of cardiomyocytes to find a suitable density for further research at which cardiomyocytes have a better growth and beating status.

We cultured respectively 4 wells of cardiomyocytes at four densities, 12k, 15k, 17k, and 25k cells/well. The results of cardiomyocytes growth and beating are shown in **Fig. 5**(A) and (B). From the CV curves of four densities of cardiomyocytes, it can be concluded that 17k cells/well have a less dispersion degree than that of 12k, 15k, and 25k cells/well, indicating that cells at 17k cells/well has high consistency. Moreover, cardiomyocytes at 17k cells/well have better beating status compared with 12k, 15k, and 25k cells/well (**Fig. 5**(C) and (D)), 17k cells/well occurs to beat earlier, and the beating rates and amplitudes were higher than cardiomyocytes at other densities. Besides, typical beating signals of cardiomyocytes at four densities are shown in **Fig. S1**. Beating signals at density of 17k cells/well at 32 h, 40 h and 46 h had similar beating rate and beating amplitude which indicate that the signals have better consistency than that at densities of 12k, 15k and 25k cells/well. Therefore, 17k cells/well we selected as the seeding density to construct the CIB.

Fig. 4

Fig. 5

Cellular growth and beating experiments

The cellular growth and beating experiments were carried out to verify CIB detection instrument. Rat cardiomyocytes with density of 17k cells/well were cultured in CIB units in the CO_2 incubator for 48h. After the cells were cultured, the CIB detection instrument began the experiment for long-term detection and high-speed detection simultaneously. According to the working principle, the impedance of CIBs increased due to cellular adhesion, proliferation and growth. **Fig. 6**(A) displays the cellular growth curves of cardiomyocytes measured by CIB detection instrument. Initially, since no cells attach on the CIB electrodes, and CI values are all zero. In the first hour which is the period of cellular adhesion, CI values increased sharply. Subsequently, CI values increased gently and stably which is mainly caused by the growth of cardiomyocytes. Images of CIB sensor are shown in **Fig. 6**(B) (C) before and after cardiomyocytes loading onto it.

For further study on the beating status of cardiomyocytes, 20 s data are recorded with high-speed sampling for cardiomyocyte beating status. In this way, typical signals of cardiomyocytes at 12 h and 40 h are shown in the inset of **Fig. 6**(A). Cardiomyocytes at 12 h had no beating signals and signals from all channels with a low noise while cardiomyocytes at 40 h had stable and strong-amplitude.

Fig. 6

Cytotoxicity and Cellular Cardiology Research

Cytotoxicity detection is an important function of CIB *in vitro*. The cytotoxicity and cell death experiments are carried out under a typical marine toxin okadaic acid (OA) for toxicity evaluation using the CIB detection system. OA can strongly inhibit protein serine/threonine phosphatase in the protein dephosphorylation which may cause cell death[53]. Neuro-2a cells are inoculated onto sensor chips with density of 10k cells/well and different concentrations of OA toxin including 25, 40, 60, 80, 100 μg/L were selected in cytotoxicity experiments. As shown in **Fig. 7**, the normalized CI values of Neuro-2a cells showed fairly consistent validities before adding OA toxin but represented obvious differences under different concentrations of OA toxin after adding the toxin. Compared with the control group, the other curves of cells with OA toxin represented different degrees of decline corresponding to the OA concentration. Therefore, the OA toxicity can be detected by the multifunction CIB system.

Fig. 7

Moreover, the multifunction CIB system is employed for the cardiomyocyte beating status, which is based on excitation-contraction (E-C) coupling. To test the performance of cardiomyocyte-based biosensor, verapamil is chosen as one of test compound . Verapamil is an L-type calcium channel blocker of the phenylalkylamine class, which can block the calcium channel and decrease the calcium influx, resulting in the decreasing impulse conduction and increasing atrio-ventricular nodal refractory period[54]. So beating rate will decline after the verapamil treatment. To verify that whether beating signals measured by our CIB detection instrument were consistent with the verapamil effect. Cardiomyocyteswere added different concentrations (0.0625, 0.13, 0.25, 0.50, 1.00, and 2.00 μM) of verapamil medium (shown in **Fig. 8**) after 40 h. **Fig. 8**(A) is the cellular growth curves of cardiomyocytes before and after adding the compound. From the cellular growth curves, verapamil has no effect on cardiomyocytes growth. The typical beating signals were shown in **Fig. 8**(B).

Compared with control group, cardiomyocytes in high concentration groups stopped beating after adding compound. The cardiomyocyte beating took long time to recovery under the verapamil treatment. In order to present the changes relative to the control group, every point of the control group was selected standard data and normalized data were displayed in **Fig. 8**(C) and (D). Compared with the control group, beating rate and amplitude of experimental groups decrease intensely after adding verapamil and present concentration-dependent recovery. Higher concentration verapamil resulted in slower recovery. From the results above, data recorded by our CIB detection instrument reflected verapamil effect of decreasing ventricular rate.

Fig. 8

In addition, a typical calcium channel agonist bay K8644 is chosen as another compound for our experiment. Bay K8644 is a potent, direct acting, voltage-sensitive calcium channel activator which may increase the calcium influx resulting in the increased beating rate[55]. In the experiment, six concentrations (2.50nM, 5.00nM, 10.00nM, 20nM, 40nM, 80nM) of Bay K8644 were added to the CIB units with cardiomyocytes which were cultured for 40h and represented regular beating signals. As is shown in **Fig. 9**(A), bay K8644 has no toxic effects on cardiomyocytes for the consistent increasing cellular growth curves at all concentrations. However, from **Fig. 9**(B) and (C), the beating rates of cardiomyocytes at all concentrations of bay K8644 suffered a sudden increase shortly after compound treatment. Meanwhile, the amplitude of beating signals dropped apparently in **Fig. 9**(D). The standard deviation of beating rate and amplitude curves of cells over 10nM were much bigger than that of cells at lower concentrations 10 hours after adding the compound. Corresponding to the beating status snapshot, we could conclude that cardiomyocytes at lower concentrations as 2.50 nM and 5.00 nM recovered to regular beating rhythm while cells at higher concentrations suffered from abnormal beating in different degrees. Therefore, the CIB detection system can reflect the effect of bay K8644. Besides, a slow delayed rectifier potassium channel blocker (chromanol 293B) and a typical anti-cancer drug (adriamycin), were performed for cardiotoxicity assessment. Results indicate that CIB system can reflect the cardiotoxicity of the two compound (**Fig. S2** and **S3** in supplementary material).

Fig. 9

Conclusion

In this study, a multifunctional cell-based impedance biosensor system was developed for early analysis of cardiovascular drug and marine toxin. The performance and function of the CIB system was tested and verified. Furthermore, experiments on four heart-related compounds and one marine toxin were carried out as an initial attempt for early screening *in vitro*. Results showed that the multifunctional CIB system can assessment the compound effect and toxicity *in vitro* by the cell-based biosensor. With the development of sensor technology and cell culture, the multifunctional cell-based impedance biosensor system may provide a utility platform for early screening of cardiovascular drug and marine toxin.

Acknowledgement

This work was supported by Major International Cooperation Project of Natural Science Foundation of China (No. 61320106002), Marine Public Welfare Project of China (No. 201305010), National Natural Science Foundation of China (No. 31228008), High-level Personnel Training Project of Cooperation Improvement of America and Oceania Region (No. 20142029), and China Postdoctoral Science Foundation (No. 2015M570511).

References

1. S. R. Braam, L. Tertoolen, A. van de Stolpe, T. Meyer, R. Passier and C. L. Mummery, Stem cell research, 2010, 4, 107-116.
2. M. A. Giorgi, R. Bolanos, C. D. Gonzalez and G. Di Girolamo, Current drug safety, 2010, 5, 54-57.
3. A. J. Moss and R. S. Kass, Journal of Clinical Investigation, 2005, 115, 2018-2024.
4. J. Bowes, A. J. Brown, J. Hamon, W. Jarolimek, A. Sridhar, G. Waldron and S. Whitebread, Nature Reviews Drug Discovery, 2012, 11, 909-922.
5. H. Laverty, C. Benson, E. Cartwright, M. Cross, C. Garland, T. Hammond, C. Holloway, N. McMahon, J. Milligan and B. Park, British journal of pharmacology, 2011, 163, 675-693.
6. C. Lawrence, C. Pollard, T. Hammond and J. P. Valentin, British journal of pharmacology, 2008, 154, 1516-1522.
7. A. Natarajan, M. Stancescu, V. Dhir, C. Armstrong, F. Sommerhage, J. J. Hickman and P. Molnar, Biomaterials, 2011.
8. L. Xiao, Z. Hu, W. Zhang, C. Wu, H. Yu and P. Wang, Biosens. Bioelectron., 2010, 26, 1493-1499.
9. S. B. Kim, H. Bae, J. M. Cha, S. J. Moon, M. R. Dokmeci, D. M. Cropek and A. Khademhosseini, Lab Chip, 2011, 11, 1801-1807.
10. K. Cusick and G. S. Sayler, Mar. drugs, 2013, 11, 991-1018.
11. J.-H. Chen, R.-C. Yu, Y. Gao, F.-Z. Kong, Y.-F. Wang, Q.-C. Zhang, Z.-J. Kang,

T. Yan and M.-J. Zhou, Food Addit. Contam. A, 2013, 30, 1933-1945.

12. M. Wiese, P. M. D'agostino, T. K. Mihali, M. C. Moffitt and B. A. Neilan, Mar. drugs, 2010, 8, 2185-2211.
13. J. van Meerloo, G. J. Kaspers and J. Cloos, in Cancer Cell Culture, Springer, 2011, pp. 237-245.
14. M. Okumura, H. Tsuzuki and B.-I. Tomita, Toxicon, 2005, 46, 93-98.
15. E. Cañete and J. Diogène, Toxicon, 2008, 52, 541-550.
16. P. Wang, G. Xu, L. Qin, Y. Xu, Y. Li and R. Li, Sensors and Actuators B: Chemical, 2005, 108, 576-584.
17. Q. Liu, C. Wu, H. Cai, N. Hu, J. Zhou and P. Wang, Chemical Reviews, 2014, 114, 6423-6461.
18. G. Xu, X. Ye, L. Qin, Y. Xu, Y. Li, R. Li and P. Wang, Biosensors and Bioelectronics, 2005, 20, 1757-1763.
19. P. Wang and Q. Liu, Cell-based biosensors: principles and applications, Artech House, Norwood, MA, 2010.
20. G. Xu, Y. Wu, R. Li, P. Wang, W. Yan and X. Zheng, Chinese Science Bulletin, 2002, 47, 1849-1856.
21. C. Ziegler, Fresenius. J. Anal. Chem., 2000, 366, 552-559.
22. C. Corcoran and G. Rechnitz, Trends Biotechnol., 1985, 3, 92-96.
23. J. Pancrazio, J. Whelan, D. Borkholder, W. Ma and D. Stenger, Amer. J. Prev. Med., 1999, 27, 697-711.
24. D. A. Stenger, G. W. Gross, E. W. Keefer, K. M. Shaffer, J. D. Andreadis, W. Ma

and J. J. Pancrazio, Trends Biotechnol., 2001, 19, 304-309.

25. I. Giaever and C. Keese, Proc. Nat. Acad. Sci. Usa., 1984, 81, 3761.
26. I. Giaever and C. R. Keese, Proceedings of the National Academy of Sciences of the United States of America, 1984, 81, 3761-3764.
27. I. Giaever and C. R. Keese, Nature, 1993, 366, 591-592.
28. I. Giaever and C. R. Keese, Biomedical Engineering, IEEE Transactions on, 1986, 242-247.
29. I. Giaever and C. R. Keese, Proceedings of the National Academy of Sciences of the United States of America, 1991, 88, 7896-7900.
30. C. Keese, N. Karra, B. Dillon, A. Goldberg and I. Giaever, In vitro toxicology, 1998, 11, 183-192.
31. C. R. Keese and I. Giaever, 1990.
32. C. R. Keese and I. Giaever, Engineering in Medicine and Biology Magazine, IEEE, 1994, 13, 402-408.
33. C. R. Keese, J. Wegener, S. R. Walker and I. Giaever, Proceedings of the National Academy of Sciences of the United States of America, 2004, 101, 1554-1559.
34. T. J. van Duijn, E. C. Anthony, P. J. Hensbergen, A. M. Deelder and P. L. Hordijk, Journal of Biological Chemistry, 2010, 285, 20137-20146.
35. P. O. Bagnaninchi and N. Drummond, Proceedings of the National Academy of Sciences, 2011, 108, 6462-6467.
36. W. Jiang and K. Harding, Google Patents, 2012.

37. M. Thakur, K. Mergel, A. Weng, S. Frech, R. Gilabert-Oriol, D. Bachran, M. F. Melzig and H. Fuchs, Biosensors and Bioelectronics, 2012.

38. L. Ceriotti, J. Ponti, F. Broggi, A. Kob, S. Drechsler, E. Thedinga, P. Colpo, E. Sabbioni, R. Ehret and F. Rossi, Sensors and Actuators B: Chemical, 2007, 123, 769-778.

39. J. Wegener, D. Abrams, W. Willenbrink, H.-J. Galla and A. Janshoff, Biotechniques, 2004, 37, 590-597.

40. A. J. Engler, C. Carag-Krieger, C. P. Johnson, M. Raab, H.-Y. Tang, D. W. Speicher, J. W. Sanger, J. M. Sanger and D. E. Discher, Journal of cell science, 2008, 121, 3794-3802.

41. K. Wilson, M. Das, K. J. Wahl, R. J. Colton and J. Hickman, PloS one, 2010, 5, e11042.

42. Y. Zhao and X. Zhang, Sensors and Actuators A: Physical, 2006, 125, 398-404.

43. A. Ahola, A. Kiviaho, K. Larsson, M. Honkanen, K. Aalto-Setala and J. Hyttinen, BioMedical Engineering OnLine, 2014, 13, 39.

44. G. Gaudesius, M. Miragoli, S. Thomas and S. Rohr, Circ Res, 2003, 93, 421 - 428.

45. B. Ben-Gigirey, M. L. Rodríguez-Velasco and A. Gago-Martínez, Journal of AOAC International, 2012, 95, 111-121.

46. A. D. Turner, R. G. Hatfield, M. Rapkova, W. Higman, M. Algoet, B. A. Suarez-Isla, M. Cordova, C. Caceres, J. van de Riet and R. Gibbs, Analytical and bioanalytical chemistry, 2011, 399, 1257-1270.

47. J. Paredes, S. Becerro, F. Arizti, A. Aguinaga, J. Del Pozo and S. Arana, Biosensors and Bioelectronics, 2012, 38, 226-232.

48. L. Wang, H. Wang, K. Mitchelson, Z. Yu and J. Cheng, Biosensors and Bioelectronics, 2008, 24, 14-21.

49. Q. Liu, C. Wu, H. Cai, N. Hu, J. Zhou and P. Wang, Chemical Reviews, 2014.

50. L. Wang, H. Wang, L. Wang, K. Mitchelson, Z. Yu and J. Cheng, Biosensors and Bioelectronics, 2008, 24, 14-21.

51. T. Wang, N. Hu, J. Cao, J. Wu, K. Su and P. Wang, Biosensors and Bioelectronics, 2013, 49, 9-13.

52. D. M. Bers, Nature, 2002, 415, 198-205.

53. T. Suzuki, A. Miyazono, K. Baba, R. Sugawara and T. Kamiyama, Harmful Algae, 2009, 8, 233-238.

54. P. Iannetti, A. Spalice and P. Parisi, Epilepsia, 2005, 46, 967-969.

55. A. Zahradníková, I. Minarovič and I. Zahradník, Journal of Pharmacology and Experimental Therapeutics, 2007, 322, 638-645.

Figure Captions

Fig. 1 (A) Equivalent circuit model of IDEs with cells growing on the sensor. (B) Equivalent circuit model of IDEs without cells. (C) Equivalent circuit model of two branches IDEs with cells growing on the sensor. R_{sol} is the spreading resistance of cell culture medium, C_{cell} is the capacitance of the cells which attached on the electrodes, R_{cell} is the resistance of the gaps between adjacent cells, R_{gap} and C_{gap} is the gap resistance and gap capacitance between cells and electrode surface, C_D is the double layer capacitance. Working principle of cellular growth (D) and cardiomyocytes beating (E) detection using CIB.

Fig. 2 (A) Fabrication processes of IDEs. (B) Layout of single IDEs. (C) The system structure of the CIB detection instrument: cell-based impedance biosensor units, hardware module, and data processing module.

Fig. 3 Detection system performance test of 50Ω (A) and 1000Ω (B). Curves in different colors represented all 16 wells of a CIB unit. (C) Sensor performance test of a CIB unit with phosphate buffer solution (PBS, pH=7.4).

Fig. 4 Cellular growth curves of Neuro-2a cells with density from 1k to 60k cells/well.

Fig. 5 (A) Cellular growth curves of rat cardiomyocytes with density from 12k to 25k cells/well. (B) The coefficient of variation curves shows the consistency of cellular growth curves during the cardiomyocytes density experiment. The statistical beating rate (C) and beating amplitude (D) results of cardiomyocytes with four densities.

Fig. 6 (A) Cellular growth curve of rat cardiomyocytes at 17k cells/well and typical beating signal at 12 and 40 h, respectively. Images of CIB sensor before (B) and after

(C) cardiomyocytes loading onto it.

Fig. 7 Cellular growth curves of Neuro-2a cells responses to different concentrations of okadaic acid (OA).

Fig. 8 Typical cardiomyocytes status response to verapamil. (A) Cardiomyocytes cellular growth curves under verapamil at concentrations from 62.5nM to 2.00μM. (B) Beating status snapshot before and after adding verapamil. (C) Normalized beating rate statistics results before and after adding verapamil. (D) Normalized amplitude statistics results before and after adding verapamil.

Fig. 9 Typical cardiomyocytes status response to bay K8644. (A) Cardiomyocytes cellular growth curves under bay K8644 at concentrations from 2.50nM to 80nM. (B) Beating status snapshot before and after adding bay K8644. (C) Normalized beating rate statistics before and after adding bay K8644. (D) Normalized amplitude statistics before and after adding bay K8644.

The system structure of the CIB detection instrument: cell-based impedance biosensor units, hardware module, and data processing module.

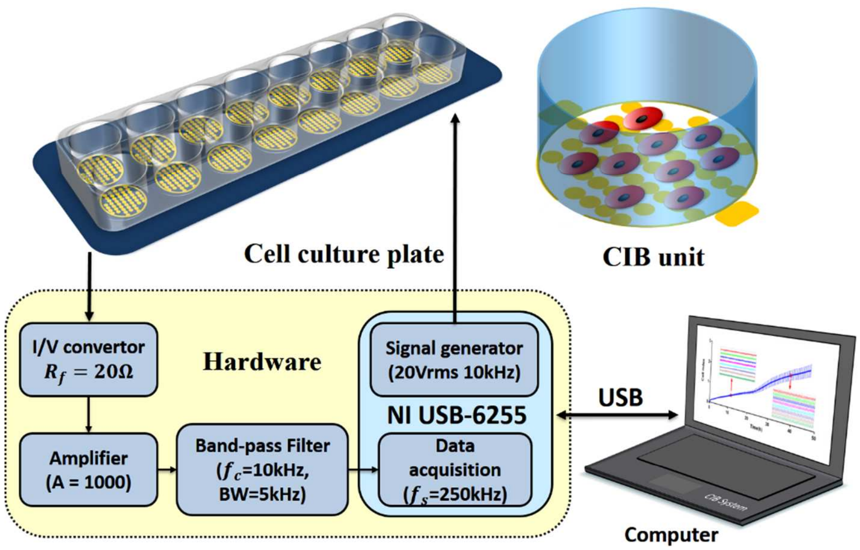

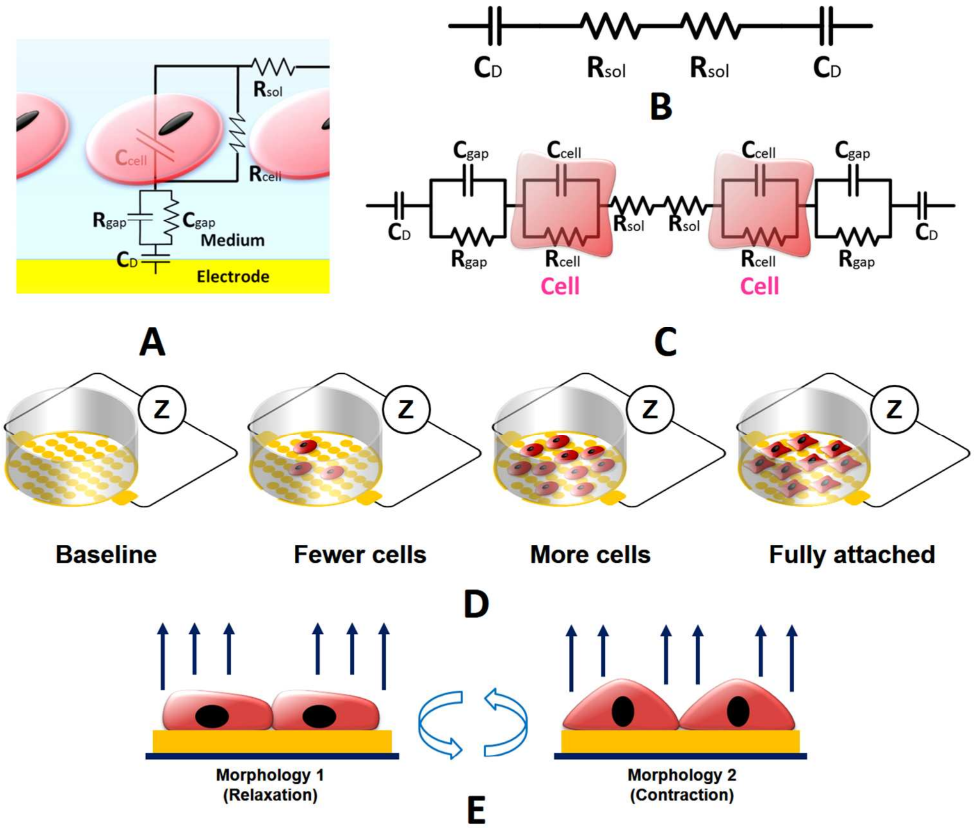

Fig. 1 (A) Equivalent circuit model of IDEs with cells growing on the sensor. (B) Equivalent circuit model of IDEs without cells. (C) Equivalent circuit model of two branches IDEs with cells growing on the sensor. Rsol is the spreading resistance of cell culture medium, Ccell is the capacitance of the cells which attached on the electrodes, Rcell is the resistance of the gaps between adjacent cells, Rgap and Cgap is the gap resistance and gap capacitance between cells and electrode surface, CD is the double layer capacitance. Working principle of cellular growth (D) and cardiomyocytes beating (E) detection using CIB.

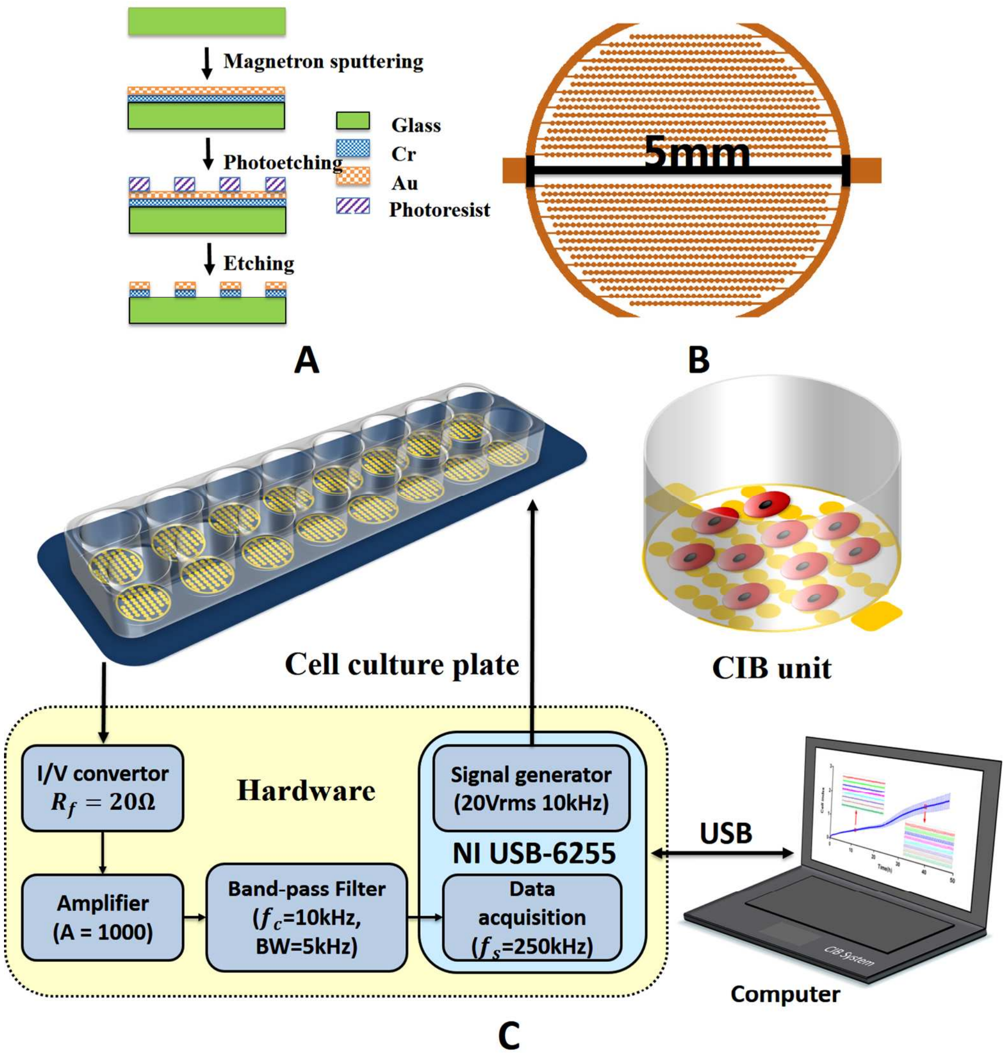

Fig. 2 (A) Fabrication processes of IDEs. (B) Layout of single IDEs. (C) The system structure of the CIB detection instrument: cell-based impedance biosensor units, hardware module, and data processing module.

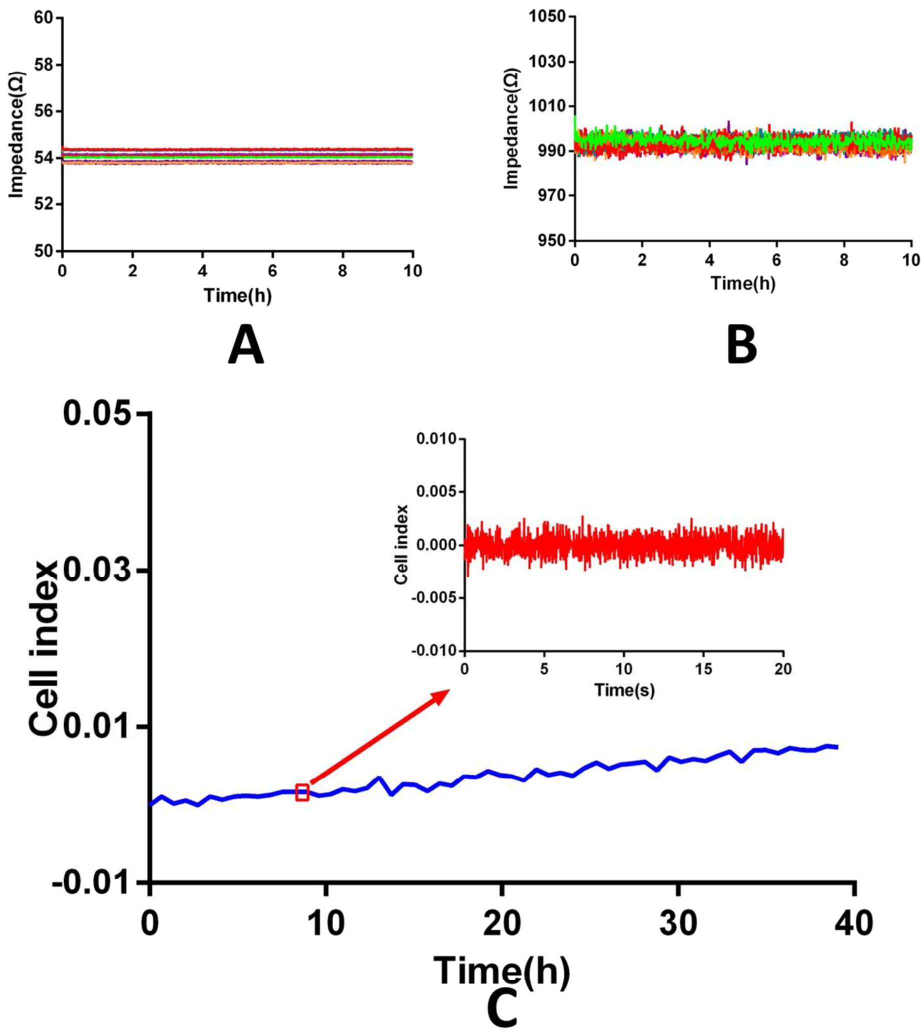

Fig. 3 Detection system performance test of 50Ω (A) and 1000Ω (B). Curves in different colors represented all 16 wells of a CIB unit. (C) Sensor performance test of a CIB unit with phosphate buffer solution (PBS, pH=7.4).

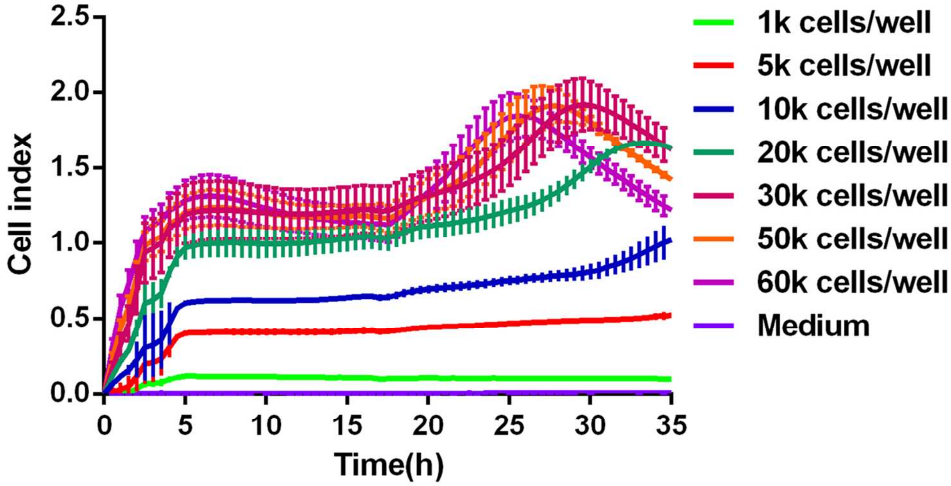

Fig. 4 Cellular growth curves of Neuro-2a cells with density from 1k to 60k cells/well.

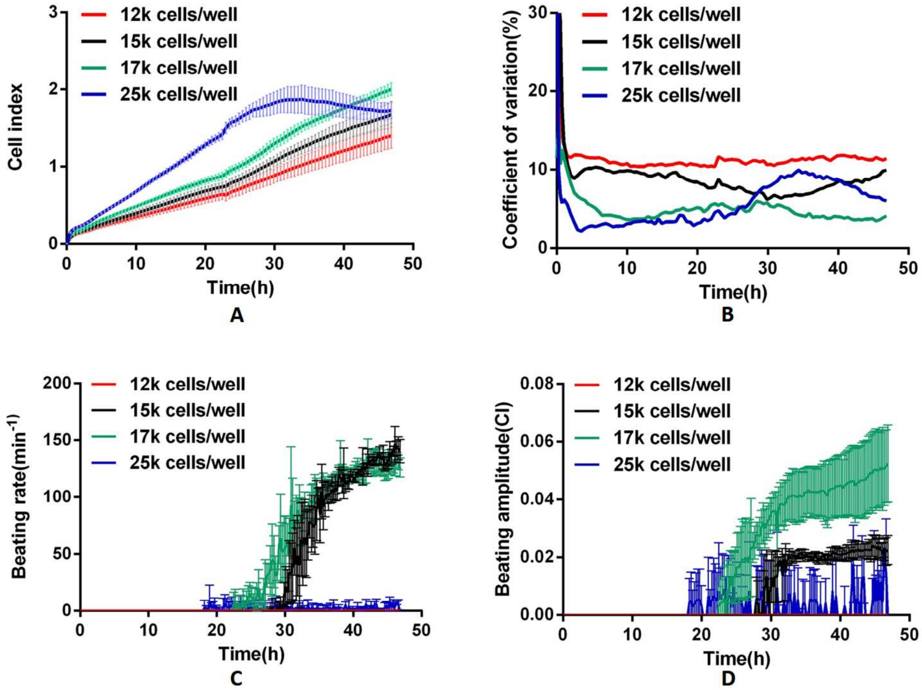

Fig. 5 (A) Cellular growth curves of rat cardiomyocytes with density from 12k to 25k cells/well. (B) The coefficient of variation curves shows the consistency of cellular growth curves during the cardiomyocytes density experiment. The statistical beating rate (C) and beating amplitude (D) results of cardiomyocytes with four densities.

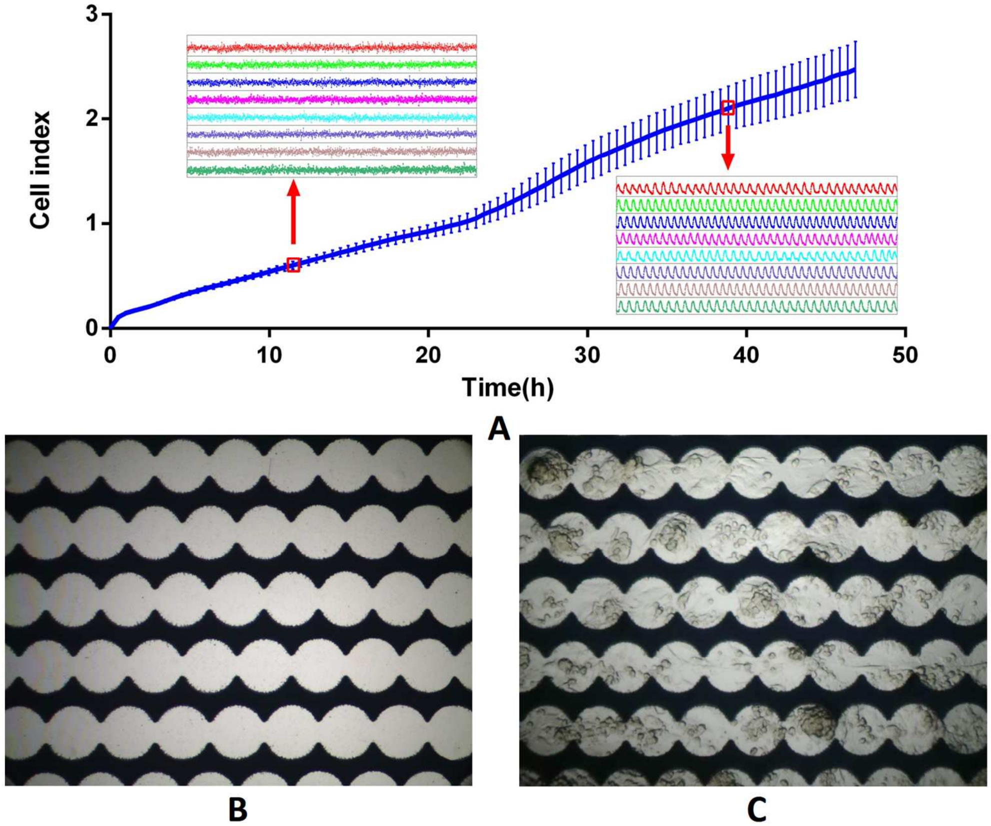

Fig. 6 (A) Cellular growth curve of rat cardiomyocytes at 17k cells/well and typical beating signal at 12 and 40 h, respectively. Images of CIB sensor before (B) and after (C) cardiomyocytes loading onto it.

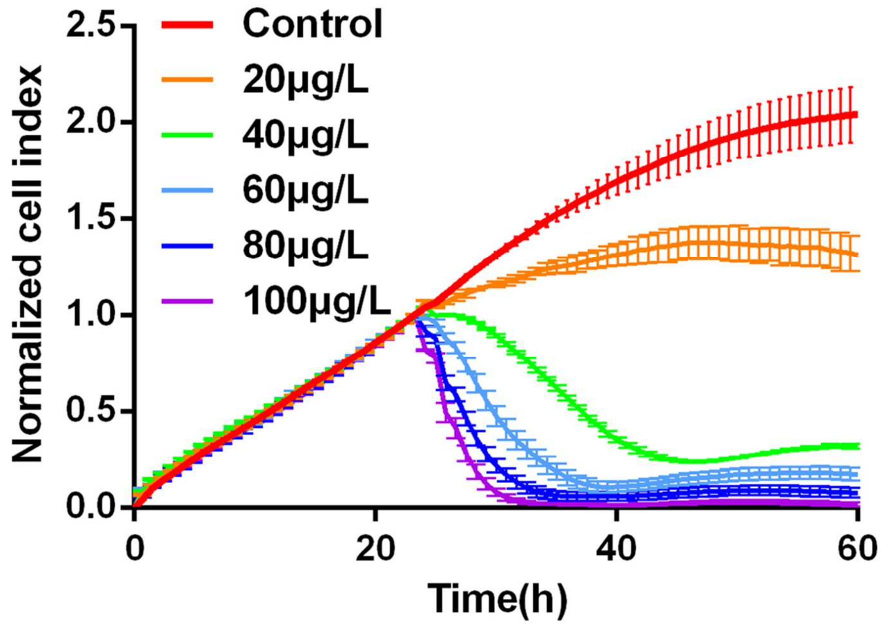

Fig. 7 Cellular growth curves of Neuro-2a cells responses to different concentrations of okadaic acid (OA).

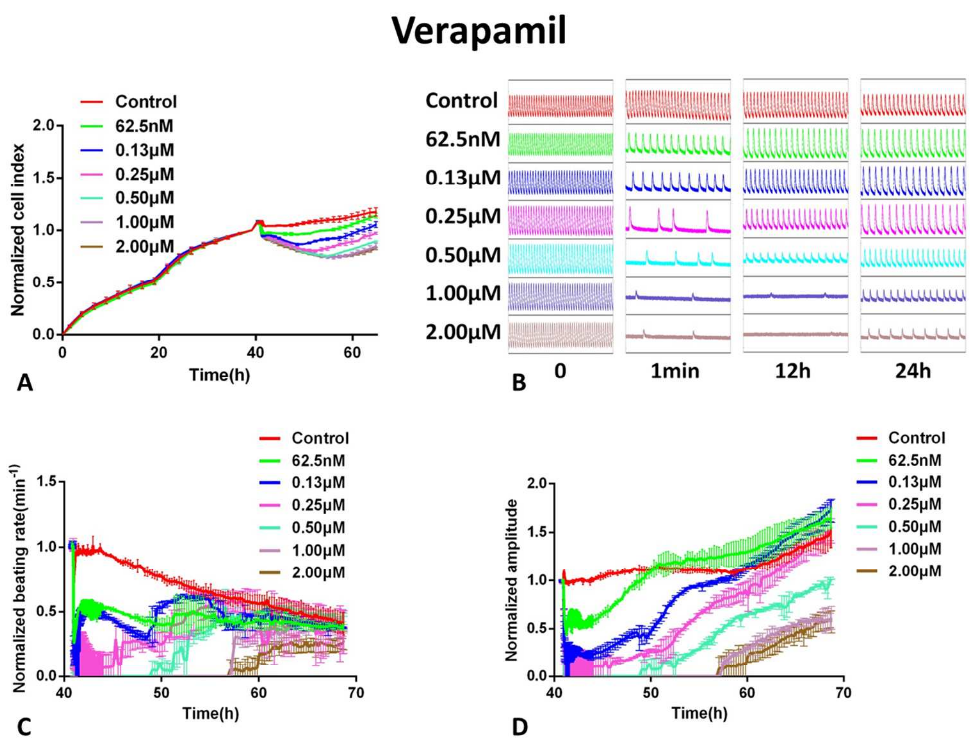

Fig. 8 Typical cardiomyocytes status response to verapamil. (A) Cardiomyocytes cellular growth curves under verapamil at concentrations from 62.5nM to 2.00μM. (B) Beating status snapshot before and after adding verapamil. (C) Normalized beating rate statistics results before and after adding verapamil. (D) Normalized amplitude statistics results before and after adding verapamil.

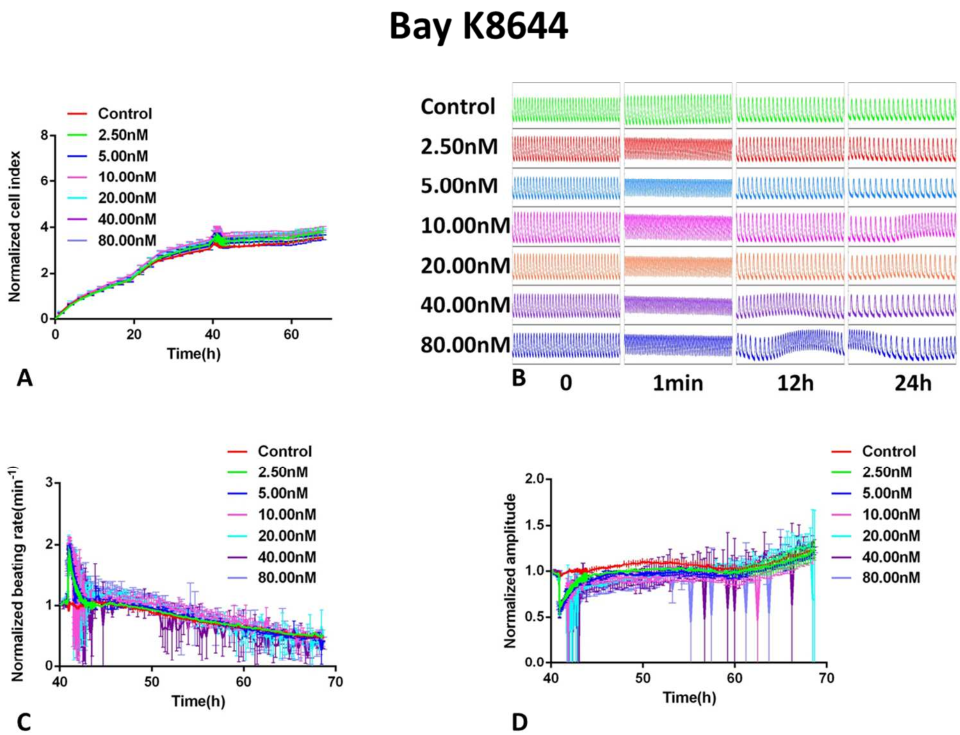

Fig. 9 Typical cardiomyocytes status response to bay K8644. (A) Cardiomyocytes cellular growth curves under bay K8644 at concentrations from 2.50nM to 80nM. (B) Beating status snapshot before and after adding bay K8644. (C) Normalized beating rate statistics before and after adding bay K8644. (D) Normalized amplitude statistics before and after adding bay K8644.